Molecular open shell configuration interaction calculations using the Dirac–Coulomb Hamiltonian

Visser, O.; Visscher, L.; Aerts, P. J. C.; Nieuwpoort, W. C.

Published in:
Journal of Chemical Physics

DOI:
10.1063/1.461987

Publication date:
1992

Molecular open shell configuration interaction calculations using the Dirac–Coulomb Hamiltonian: The f^6-manifold of an embedded EuO_6^{9-} cluster

O. Visser, L. Visscher, P. J. C. Aerts, and W. C. Nieuwpoort

Citation: The Journal of Chemical Physics **96**, 2910 (1992); doi: 10.1063/1.461987
View online: https://doi.org/10.1063/1.461987
View Table of Contents: http://aip.scitation.org/toc/jcp/96/4
Published by the American Institute of Physics

Molecular open shell configuration interaction calculations using the Dirac–Coulomb Hamiltonian: The f^6-manifold of an embedded EuO_6^{9-} cluster

O. Visser, L. Visscher, P. J. C. Aerts, and W. C. Nieuwpoort
Laboratory of Chemical Physics and Materials Science Centre, University of Groningen, Nijenborgh 16, 9747 AG Groningen, The Netherlands

(Received 25 October 1991; accepted 15 November 1991)

We present results of all-electron molecular relativistic (Hartree–Fock–Dirac) and nonrelativistic (Hartree–Fock) calculations followed by a complete open shell configuration interaction (COSCI) calculation on an EuO_6^{9-} cluster in a Ba_2GdNbO_6 crystal. The results include the calculated energies of a number of states derived from the f^6 — manifold and ^5D–^7F luminescence transition wavelengths. The calculations were performed using the molecular Fock–Dirac (MOLFDIR) program package developed in our laboratory. The theory and methods employed in this package are briefly described. The physical models used to analyze the Eu^{3+} impurity states range from a bare Eu^{3+} ion to an EuO_6^{9-} cluster embedded in a Madelung potential representing the rest of the crystal. We show that it is necessary to use the embedded cluster model to get a reasonable description of the crystal field splittings of the states arising from the f^6-manifold. Our results indicate that the calculated splittings are very sensitive to the orbitals used. It is therefore essential that relativistic orbitals be used from the outset.

I. INTRODUCTION

Compounds containing lanthanide ions ($Z = 57$–71) form an interesting class of materials, both from a scientific and a practical point of view. Their optical and magnetic properties for example are at present technically widely exploited, while being subjects of continuing experimental and theoretical investigations. These properties arise from the complex manifold of electronic states arising from the incompletely filled $4f$ shells of the lanthanide atoms or ions. Since the classic work of Becquerel and Bethe[1,2] it is well known how to describe these states in crystalline surroundings semiempirically. In recent years this theory has been revitalized and has considerably been extended by Thole in connection with the rationalization of x-ray absorption spectroscopic data.[3,4] At least for the lower lying electronic states, the Coulombic interaction between the electrons (on the order of eVs) still dominates the spin–orbit interaction (on the order of tenths of eVs), although not as heavily as in the case of the $3d$ metals. In contrast to the latter case, however, the perturbing effects of the surrounding are much smaller than the spin–orbit interaction and therefore smaller than relativistic effects in general. This poses a serious problem when one wants to go beyond a semiempirical description and use *ab initio* computational methods, for example, to obtain more quantitative insight into the origin of crystal fields or into the rates of various radiative or nonradiative decay or excitation transfer processes. The problem is whether *ab initio* results based on the nonrelativistic Schrödinger equation with relativistic corrections added on can be relied upon or that a relativistic approach is needed from the outset to account for the differences between relativistic and nonrelativistic orbitals.

At present the *ab initio* treatment of relativistic effects in compounds of the kind considered here is limited to the use of an effective Schrödinger equation for valence electrons containing relativistic perturbation terms and a relativistic core potential derived from atomic Fock–Dirac calculations (Ref. 5 and references therein). As it is based on a Schrödinger equation this useful approach allows the inclusion of electron correlation effects by standard quantum chemical methods. All electron *ab initio* calculations, however, including relativistic effects as well as correlation effects on the same theoretical level, have not yet been performed on molecular systems containing heavy atoms. Some calculations based on relativistic quantum mechanics have been performed (Refs. 6–8 and references therein). Most of the calculations concern atoms, and a few deal with diatomic molecules. Applications to molecular systems containing more than two nuclei have been sparse,[9–12] except for calculations based on a local density approach.

More than a decade ago van Piggelen[13] has carried out nonrelativistic *ab initio* calculations, with spin–orbit perturbation corrections, to describe some of the states from the f-manifold of the Eu^{3+} impurity in Ba_2GdNbO_6, using a molecular model (an EuO_6^{9-} cluster embedded in the Madelung field of the rest of the crystal). The impurity site in this compound has cubic (octahedral) symmetry, which was important to make the calculations feasible. His interpretation of the calculated crystal field splitting was inconclusive because of the problem mentioned. In this work we use the same molecular model but carry out fully relativistic calculations by applying the all-electron Hartree–Fock–Dirac method followed by relativistic configuration interaction (CI), resulting in a complete intermediate coupling description of the f-like manifold of the lanthanide impurity. One aim of the work is to obtain results that can serve as a reference for more approximate methods. The method also enables the study of correlation effects and the effects of the Breit interaction.[11]

 0021-9606/92/042910-10$06.00

II. THEORY

We use an average of configurations self-consistent-field (SCF) method (Hartree–Fock for nonrelativistic calculations, Hartree–Fock–Dirac for relativistic calculations) to generate a set of one-electron spin orbitals. Using these average orbitals, we perform a complete open shell configuration interaction (COSCI) calculation to get a description of the open shell manifold. In this section we give the basic equations of the method and the way these are solved. Some details of the molecular Fock–Dirac (MOLFDIR) program package[9,11,14,15] are given, in particular the form of the basis functions, kinetic and atomic balance, and general contraction.

A. General

The time-independent Dirac equation for one-electron molecular systems[16,17] is given by

$$h\varphi = \varepsilon\varphi, \tag{1}$$

in which h is the one-electron Dirac operator defined by

$$h = c\alpha\cdot\mathbf{p} + (\beta - 1)mc^2 + V. \tag{2}$$

We have shifted the energy scale by $-mc^2$ to facilitate comparison with nonrelativistic energies. The α and β are 4×4 matrices defined by

$$\alpha = \begin{pmatrix} 0 & \sigma \\ \sigma & 0 \end{pmatrix}$$

and

$$\beta = \begin{pmatrix} 1 & 0 \\ 0 & -1 \end{pmatrix} \tag{3}$$

in which σ is the collection of Pauli spin-matrices, V is the potential energy $V(\mathbf{r};\mathbf{R})$ due to the nuclei at $\mathbf{R}$, c is the speed of light in vacuum (137.036 02 a.u. used), and m is the rest-mass of the electron. $\varphi(\mathbf{r})$ is a four-component spinor, conveniently written in bispinor form,

$$\varphi = \begin{pmatrix} \varphi^L \\ \varphi^S \end{pmatrix}. \tag{4}$$

The first-order approximation to the positive-energy state is

$$\varphi^S \approx \frac{1}{2mc}\,\sigma\cdot\mathbf{p}\varphi^L \tag{5}$$

so the lower bispinor is conventionally called the "small component," and the upper bispinor is the "large component."

One can generalize the one-electron Dirac equation to an approximate relativistic many-electron equation (the Dirac–Coulomb equation),[18] which is given (in atomic units) by

$$\left\{\sum_i \left[\alpha_i\cdot\mathbf{p}_i + (\beta_i - 1)mc^2 + V_i\right] + \sum_{i<j}\frac{1}{r_{ij}}\right\}\psi = E\psi. \tag{6}$$

The two-electron interaction in this equation consists of the usual Coulomb term and is not relativistically invariant; the leading correction to the two-electron interaction (the Breit interaction[19]) can be included either variationally or by perturbation theory,[9,20,21] but has been left out in this work.

B. Open shell approach

The molecules or clusters, modeling bulk or surface properties of solids, we want to study contain heavy atoms and are in general open shell systems. Especially lanthanides and actinides have an open f-shell, which gives rise to a large number of energy eigenstates lying close together. A simple open shell SCF method alone is not sufficient to describe such a manifold. First, significant interaction between the Russell–Saunders terms of the f-multiplet should be expected. Second, since (as is generally known) the correct eigenfunctions of the Dirac–Coulomb Hamiltonian are neither pure LS-coupled functions nor pure JJ-coupled functions, a many-electron function in intermediate coupling should be constructed. This can be accomplished by forming linear combinations of determinants constructed from LS or JJ-coupled one-electron spinors. Furthermore, since we are interested in the optical spectrum of the f-manifold, we need to calculate a large number of the energy eigenstates. A separate SCF calculation for each of these states is cumbersome, and is certainly not a practical approach.

By using the COSCI approach these problems can be solved. We start with a SCF calculation using an average energy expression [defined as the average of the energy expressions for all possible individual states of the relevant configuration(s)], resulting in the "average" total energy and a set of "average" orbitals. Next, a CI calculation is performed within the full-CI space generated from the set of open shell orbitals from the SCF calculation. This results in a description of the open shell manifold which is not tied to one of the extreme coupling schemes.

C. The relativistic open shell SCF equations

The relativistic open shell SCF equations are formally derived in the same way as the nonrelativistic equations.[22] The one-electron Schrödinger operators are replaced by Dirac operators and the scalar orbitals are now four component spinors. Fundamentally there is of course an important difference in the meaning of the variational method since it is used to locate a stationary state in the positive energy domain instead of an absolute minimum. The resulting SCF equations are called the Hartree–Fock–Dirac equations.

The average of configuration energy expression which is used in the MOLFDIR program package has the following form:[14]

$$E = \sum_k^C h_k + \tfrac{1}{2}\sum_{kl}^C Q_{kl} + f\left[\sum_m^O h_m + \tfrac{1}{2}af\sum_{mn}^O Q_{mn} + \sum_{k,m}^{C,O} Q_{km}\right]. \tag{7}$$

In this equation, k and l label closed shell spin-orbitals (which, by definition, are occupied by one electron), m and n label open shell spin-orbitals (with related to them a fractional occupation umber f and a coupling constant a), h_k is the diagonal matrix element of the one-electron Dirac operator [from Eq. (1)] over spin-orbital φ_k, and $Q_{ij} \equiv J_{ij} - K_{ij}$ in which J_{ij} and K_{ij} are the usual Coulomb and exchange integrals. Apart from the use of four-component spin–orbitals instead of orbitals, the energy expression differs from the energy expression used by Roothaan in the detailed form of the one-electron operators (Dirac-operators vs one-electron

Schrödinger operators) and of the two-electron operators when the Breit interaction is included.

If we use the average of configuration total energy expression, the coupling constant and fractional occupation number are given as functions of the number of open shell electrons n and the number of open shell orbitals d,

$$f=\frac{n}{d}, \tag{8}$$

$$a=\frac{d(n-1)}{n(d-1)}. \tag{9}$$

For completeness, we present the working formulas which are obtained when the SCF equations are solved using a basis set (consisting of either two or four component spinors) expansion technique. In these equations p, q, r... label basis spinors χ_p, χ_q, χ_r,... and S_{pq} is the overlap between basis spinors χ_p and χ_q, and $(pq\|rs)$ is an antisymmetrized two-electron repulsion integral in charge-cloud notation,

$$\alpha=\frac{1-a}{1-f}, \tag{10}$$

$$|i\rangle=\sum_p \chi_p c_{pi}, \tag{11}$$

$$\begin{aligned} D^C_{pq}&=\sum_k^C c^*_{qk}c_{pk},\\ D^O_{pq}&=f\sum_m^O c^*_{qm}c_{pm}, \end{aligned} \tag{12}$$

$$\begin{aligned} Q^C_{pq}&=\sum_{rs}(pq\|rs)D^C_{sr},\\ Q^O_{pq}&=\sum_{rs}(pq\|rs)D^O_{sr}, \end{aligned} \tag{13}$$

$$L^C_{pq}=\sum_{rs}\left[S_{pr}D^C_{rs}Q^O_{sq}+Q^O_{pr}D^C_{rs}S_{sq}\right], \tag{14}$$

$$L^O_{pq}=\sum_{rs}\left[S_{pr}D^O_{rs}Q^O_{sq}+Q^O_{pr}D^O_{rs}S_{sq}\right],$$

$$\begin{aligned} F^C&=h+Q^C+Q^O+\alpha L^O,\\ F^O&=h+Q^C+aQ^O+\alpha L^C. \end{aligned} \tag{15}$$

For the closed shell orbitals we get the equation

$$F^C|k\rangle=\varepsilon_k|k\rangle, \tag{16}$$

and for the open shell orbitals we get the equation

$$F^O|m\rangle=\varepsilon_m|m\rangle. \tag{17}$$

Equations (16) and (17) need to be solved iteratively. The coupling operators L^C and L^O take care of the orthogonality between the closed shell and open shell solutions. We get the following expression for the total energy:

$$\begin{aligned} E=&\mathrm{Tr}[H^D D^C]+\tfrac{1}{2}\mathrm{Tr}[Q^C D^C]+\mathrm{Tr}[H^D D^O]\\ &+\tfrac{1}{2}a\,\mathrm{Tr}[Q^O D^O]+\mathrm{Tr}[Q^O D^C]. \end{aligned} \tag{18}$$

D. The COSCI method

In this section, we mention some features of the COSCI method. The many-electron function space used in the COSCI calculations is the full-CI space generated from a (small) set of active spin–orbitals which is usually chosen to be the set of open shell spin–orbitals from the SCF calculation. Since the average energy is proportional to the trace of the Hamiltonian matrix in this many-electron basis, it is invariant for unitary transformations of the one-electron basis. In particular, it does not make any difference if we had started with an LS coupled instead of a JJ coupled basis set.

Since only the open shell space is used to construct the CI matrix, correlation corrections are hardly accounted for at this stage. Also, the open shell orbitals are not optimized for individual states. The method is expected, however, to yield a balanced, global picture of the open shell manifold of states. More accurate descriptions of specific states can be found subsequently by the application of multireference configuration interaction (MRCI) or multiconfiguration self-consistent field (MCSCF) techniques.

We define the set of frozen orbitals to consist of all one-electron spinors which are present in all determinants spanning the CI-space. The interaction with these frozen orbitals is taken into account by using an effective one-electron operator h',

$$h'=h+\sum_f^F (J_f-K_f), \tag{19}$$

where J_f is the Coulomb operator with spin–orbital φ_f, K_f is the exchange operator with spin–orbital φ_f, and the summation runs over the set of frozen spin–orbitals F. The matrix elements of this operator can be calculated easily using the fact that the one-electron spinors are solutions of the SCF Eqs. (16) and (17).

Finally, it is clear that while the COSCI method has been introduced here to perform open shell calculations with a relativistic Hamiltonian, it can also be used for calculations with a nonrelativistic Hamiltonian.

E. Basis functions

The MOLFDIR package works with two distinct sets of, usually atom centered, scalar (contracted) Cartesian Gaussian functions, a large component set $\{g_i^L\}$ and a small component set $\{g_i^S\}$. The two-electron repulsion integrals are calculated over the functions belonging to these sets. From these two scalar sets, two new sets of symmetry adapted molecular basis spinors $\{\chi_l^L\}$ and $\{\chi_s^S\}$ are constructed using the Dirac double group symmetry elements. The spinors χ_l^L and χ_s^S are defined by

$$\chi_l^L=\begin{pmatrix}\chi_l^{L\alpha}\\ \chi_l^{L\beta}\\ 0\\ 0\end{pmatrix}$$

and

$$\chi_s^S=\begin{pmatrix}0\\ 0\\ \chi_s^{S\alpha}\\ \chi_s^{S\beta}\end{pmatrix}, \tag{20}$$

$$\chi_l^{L\alpha}=\sum_i g_i^L c_{il}^{L\alpha},\quad \chi_l^{L\beta}=\sum_i g_i^L c_{il}^{L\beta},$$

$$\chi_s^{S\alpha}=\sum_i g_i^S c_{is}^{S\alpha}$$

and

$$\chi_s^{S\beta} = \sum_i g_i^S c_{is}^{S\beta}, \tag{21}$$

where the coefficients $c_{ij}^{X\sigma}(X\in\{L,S\};\ \sigma\in\{\alpha,\beta\})$ in Eq. (21) are determined by symmetry. Thus, each nonzero component of these basis spinors consists of a linear combination of the basis functions from set $\{g_i^L\}$ or set $\{g_i^S\}$.

F. Kinetic balance and general contraction

As has been discussed by several authors,[23–25] it is important to ensure that the basis set in which the one-electron functions are expanded fulfills the kinetic balance condition. This condition requires that for each function χ_I^L in the large component basis, the function $\alpha\cdot\mathbf{p}\chi_I^L$ is contained in the small component basis set. Since kinetic balance is neither a necessary nor sufficient condition to produce the best approximate eigensolutions, we use an extended kinetic balance scheme.[15] In practice this means that the small component basis set contains more basis functions than those minimally required by the kinetic balance condition.

The first set of extra functions results from our choice to employ two separate primitive Gaussians instead of the fixed linear combination that results from $\alpha\cdot\mathbf{p}$ operating on a single Gaussian primitive in the large component.

A second set of extra functions is used in molecular calculations were atomic solutions are used to contract the large and small component basis functions. In addition to the kinetically balanced functions the atomic small component solutions are used as small component basis functions. A basis set which includes such an extension is called an atomically balanced basis set.[15]

When general contraction[26] is used to reduce the variational space we still require that the small component basis fulfills atomic and kinetic balance conditions. The contraction reduction is thereby counteracted by the fact that up to four contracted functions for each large component function are necessary (up to two functions to ensure kinetic balance, and up to two functions to ensure atomic balance). Although these small component functions may tend to form a linear dependent set, in which case one or more functions can be removed, the gain obtained by the use of general contraction in the small component basis set is small compared to that obtained in the large component basis set.

III. The Ba_2GdNbO_6:Eu system

A. Description of the system

In 1966, Blasse *et al.*[27,28] have obtained experimental data (luminescence spectra) on some compounds which contained an Eu^{3+} impurity. Due to the approximate validity of spin and parity selection rules, electric dipole transitions between the ^5D and ^7F levels of the Eu^{3+} impurity are forbidden in first approximation. The spin selection rule is lifted by the spin–orbit coupling. The magnetic dipole and quadrupole transitions are only forbidden by a spin selection rule, which is again lifted by the spin–orbit coupling. To investigate the effect of the symmetry of the surroundings, a series of compounds was studied, a compound in which the Eu^{3+} ion occupies a strict center of (O_h) symmetry, a compound in which small deviations from this symmetry occur, and a compound with no symmetry at all. In the last case, both electric and magnetic dipole transitions can occur, while in the first case only magnetic dipole transitions are allowed.[29,30]

We have chosen to study a compound with a strict center of symmetry, Ba_2GdNbO_6:Eu. The advantage is that calculations can be performed using O_h symmetry, which greatly reduces the computational efforts needed (both in terms of CPU time and of disk space).

The Ba_2GdNbO_6 crystal (Fig. 1) has an ordered perovskite structure.[31] The unit cell of the crystal is a cube divided in eight smaller cubes. In the center of the smaller cubes we find alternating Gd^{3+} and Nb^{5+} ions, on the corners of the smaller cubes we find Ba^{2+} ions, and at the middle of the sides of the small cubes the O^{2-} ions are positioned. The Eu^{3+} impurity occupies one of the Gd^{3+} sites with symmetry O_h. It is surrounded by six O^{2-} ions, forming an "EuO_6^{9-} cluster," with an Eu–O distance of 4.02 a.u.

The experimental results obtained by Blasse *et al.* (the energy distribution of the emission of Eu^{3+}-activated Ga_2GdNbO_6) show a sharp line at 595 nm (16 800 cm^{-1}) corresponding to the $^5D_0\rightarrow{}^7F_1$ transition. This is an allowed magnetic dipole transition. Also, at least six weak and broad lines are visible in the region 610–630 nm (15 900–16 400 cm^{-1}). These lines were assigned to the $^5D_0\rightarrow{}^7F_2$ transitions (the large number of lines is due to simultaneous vibronic transitions).

B. Physical model

We have performed all-electron average of configuration open shell Hartree–Fock and Hartree–Fock–Dirac calculations, followed by COSCI calculations [using, respectively, the Schrödinger Hamiltonian (*NR*) and the Dirac–Coulomb Hamiltonian (*FD*)], on part of the Ba_2GdNbO_6 crystal together with the impurity. This part of the material, cut from the complete system, will be referred to as "the cluster," even when "the cluster" consists of one atom only (the impurity atom). The influence of the surrounding infinite crystal is accounted for by considering the electrostatic effects on the cluster only. The Madelung potential of the

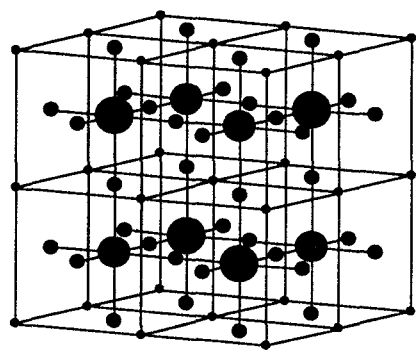

FIG. 1. The Ba_2GdNbO_6 unit cell. In order to get a better view of the structure of the cell, the ions have not been drawn to scale. Small black spheres, Ba^{2+}; small grey spheres O^{2-}, remaining large spheres, alternating Gd^{3+} and Nb^{5+}. The Eu^{3+} impurity occupies a Gd^{3+} site.

crystal (with the contributions from the atoms contained in the cluster removed) has been included in the cluster calculations. Technically, this potential was represented by a set of fitted point charges.[32]

We define three different models of the physical system of interest which successively improve on the quality of the description. (a) Eu, a bare Eu^{3+} ion. This is the crudest model available since none of the effects of the surroundings are included. (b) EuMP, an Eu^{3+} ion embedded in the Madelung potential. This model is expected to give more realistic results since the electrostatic effects of the surroundings are included in the calculation. (c) EuO_6MP, an EuO_6^{9-} cluster embedded in the Madelung potential of the rest of the crystal. In principle still larger clusters can be defined, and eventually the results from the calculations are expected to converge to the results from a hypothetical calculation on a physical crystal containing the impurity. Relativistic calculations using the Hartree–Fock–Dirac and subsequent COSCI method on systems much larger than the EuO_6^{9-} cluster are not yet technically feasible. To conclude with, we define one last model system. (d) EuO_6, a bare EuO_6^{9-} cluster. This model system is included for comparison.

IV. COMPUTATIONAL DETAILS

A. Basis sets

The primitive basis set for the Eu^{3+} ion has been optimized for the ^7F state (the ground state), starting with the Eu^{3+} basis set from van Piggelen.[33] For technical reasons (to improve the efficiency), this basis set was reoptimized under the constraint that the *d*-exponents be a subset of the *s*-exponents, and that the *f*-exponents be a subset of the *p*-exponents. This resulted in a very reasonable basis set (Table I) for the Eu^{3+} ion, 18*s*, 15*p*, 10*d*, and 8*f*.

The total energy of the ^7F ground state using this basis set is $-10\,422.003\,72$ a.u. (van Piggelen, $-10\,422.016\,87$ a.u.; numerical HF, $-10\,422.037\,88$ a.u.). The radial expectation value for *r* is given in Table II. From the table it can be seen that the basis set calculations agree in reasonable detail with the numerical calculations. The basis set optimized with the constraint on the exponents yields necessarily results that are slightly less in quality than the results of the basis set optimized without constraints. Also by a study of the *f*-spectrum later on it is concluded that the basis set is good enough for our purposes.

Based on average of configuration atomic open shell Hartree–Fock and Hartree–Fock–Dirac calculations on the Eu^{3+} ion, general contracted basis sets were constructed for the molecule. The small component basis set was constructed using atomic and kinetic balance. This procedure resulted in a $(6s,5p,3d,2f)$ nonrelativistic basis set, and in a $(6s,9p,5d,3f|10s,13p,14d,8f,5g)$ relativistic scalar basis set.

For the oxygen ion we have used a $(10s,6p)$ primitive basis set (Table I) which has been optimized (nonrelativistically) for the O^- ion.[34] Based on Hartree–Fock and Hartree–Fock–Dirac calculations on the O^{2-} ion general contracted basis sets were constructed. Again, the small component basis set was constructed using atomic and kinetic balance. This procedure resulted in a $(3s,2p)$ nonrelativistic basis set, and in a $(3s,3p|4s,4p,5d)$ relativistic scalar basis set.

TABLE I. Primitive basis sets used for Eu^{3+} and for O^{2-}.

Eu^{3+} basis			O^{2-} basis[a]	
S		4 568 512.763 856 917 6	*S*	14 362.130 2
S		684 565.009 613 808 2	*S*	2 154.845 8
S		155 804.248 861 146 2	*S*	490.333 7
S		44 117.849 426 965 2	*S*	138.568 6
S		14 377.854 466 075 4	*S*	44.851 3
S		5 174.382 955 328 0	*S*	15.849 5
S	*D*	2 003.243 622 978 9	*S*	5.863 7
S	*D*	820.694 856 558 4	*S*	1.490 0
S	*D*	350.217 442 656 9	*S*	0.561 2
S	*D*	149.892 154 564 9	*S*	0.181 3
S	*D*	68.436 172 618 3	*P*	47.592 5
S	*D*	32.067 803 890 9	*P*	10.865 7
S	*D*	15.317 827 648 8	*P*	3.259 5
S	*D*	7.127 594 808 6	*P*	1.075 6
S	*D*	3.209 811 509 9	*P*	0.341 2
S	*D*	1.322 432 897 1	*P*	0.092 7
S		0.675 479 568 3		
S		0.292 415 667 7		
P		49 422.173 251 800 0		
P		11 709.355 524 531 5		
P		3 801.203 352 874 0		
P		1 450.488 125 739 5		
P		611.759 801 185 9		
P		275.055 800 696 4		
P	*F*	128.705 424 110 5		
P	*F*	61.608 287 950 2		
P	*F*	29.237 728 903 3		
P	*F*	14.336 247 145 4		
P	*F*	6.894 638 710 6		
P	*F*	3.202 070 109 0		
P	*F*	1.433 500 509 5		
P	*F*	0.576 375 949 9		
P		0.242 306 746 8		

[a] R. Broer (unpublished).

B. Madelung potential

The crystal is taken to be purely ionic, $Ba_2^{2+}Gd^{3+}Nb^{5+}O_6^{2-}$. Using these formal charges, the Ma-

TABLE II. Expectation value of *r* (in a.u.) for several Eu^{3+} orbitals.

$\langle r \rangle$	NMCHF[a]	ASCF van Piggelen[b]	ASCF (this work)[c]
1*s*	0.024 08	0.024 08	0.024 08
2*s*	0.102 53	0.102 53	0.102 53
3*s*	0.264 42	0.264 42	0.264 43
4*s*	0.597 86	0.597 85	0.597 91
5*s*	1.452 85	1.452 70	1.452 99
2*p*	0.087 12	0.087 12	0.087 12
3*p*	0.254 55	0.254 55	0.254 55
4*p*	0.613 37	0.613 38	0.613 41
5*p*	1.606 75	1.606 31	1.607 31
3*d*	0.226 54	0.226 54	0.226 54
4*d*	0.653 12	0.653 08	0.652 95
4*f*	0.806 44	0.806 25	0.804 83

[a] NMCHF = numerical Hartree–Fock results.
[b] ASCF van Piggelen = basis set results, optimized basis set.
[c] ASCF this work = basis set results, basis set optimized under constraints.

delung potential in the cluster region has been calculated. After subtracting the cluster contributions, the remaining potential was fitted with a set of point charges. The fit results for the two different clusters (the Eu^{3+} ion, and the EuO_6^{9-} system) are given in Table III.

For the interpretation of the results it is useful to note that the Madelung potential used with the Eu^{3+} ion can be fitted with only six charges on the O^{2-} sites (at a distance of 4.02 a.u.). The fit charges are -0.865, with a standard deviation in the potential of 0.04 a.u.[13] In the embedded ion calculations, however, we have used the much more accurate fit given in Table III.

C. The EuO_6^{9-} cluster

In the Hartree–Fock–Dirac calculations on the EuO_6^{9-} clusters, using the experimental geometry, the symmetry unique two-electron integrals which were larger than 10^{-12} for the $(LL|LL)$ and $(LL|SS)$ integrals, and the 10^{-8} for the $(SS|SS)$ integrals were calculated. This resulted in 2×10^6 $(LL|LL)$ integrals, 48×10^6 $(LL|SS)$ integrals and 241×10^6 $(SS|SS)$ integrals. If no symmetry would have been employed, we would have obtained 0.1×10^9 $(LL|LL)$ integrals, 2.2×10^9 $(LL|SS)$ integrals, and 12.7×10^9 $(SS|SS)$ integrals.

We found that the convergence of the SCF iterations was very slow. Normally, the computational efforts needed for a single SCF iteration can be reduced by temporarily using only part of the large-component two-electron integrals, or by temporarily fixing the contributions of the small component two-electron integrals to the Fock matrices; in this case we found that both of these methods did seriously degrade the convergence behavior.

We also found that selection of the open shell eigenvectors by overlap with the eigenvectors of the previous iteration did not work very well for the EuO_6^{9-} systems. However, selection by character (thus forcing the open shell orbitals to be constructed from the Eu f-basis spinors) worked much better.

V. RESULTS

A. The free Eu^{3+} ion

In order to get an estimate of the accuracy which can be obtained using the given general contracted basis set together with the COSCI approach, we have performed some calculations on the Eu^{3+} ion in the nonrelativistic limit: (1) Numerical calculations using the NMCHF program of Froese-Fischer,[35] these calculations are used as reference. (2) Atomic basis set expansion calculations with the ASCF (Ref. 13) program, using the uncontracted basis set described before. (3) MOLFDIR–COSCI calculations using the general contracted basis set. The results are given in Table IV. All absolute energies are too high by ~0.034 a.u., due to the finite basis set approximation. The relative errors show the accuracy within the f-manifold, which is in general much better than 10^{-3} a.u. For the ^7F and ^5L-states, the error due to the use of a set of average orbitals (column III − column II in Table IV) is significantly larger than for the other states. This error, especially in case of the ^5L-state, is partially canceled by the basis set error (column II − column I in Table IV).

We conclude that in the worst case the accuracy of the calculations, as far as splittings *between* Russell–Sauders term are concerned, can be as bad as 3×10^{-3} a.u. (~600 cm^{-1}), and that this is mainly due to the average f-shell approach. The accuracy in the many-electron total energies will therefore not significantly be improved by using a more flexible basis set. The splittings within Russell–Saunders terms due to relativistic and ligand field effects are much smaller, and the absolute accuracy of these splittings is expected to be much better.

TABLE III. Fit to the Madelung potential for several clusters. Position = position of the fit-charges in units of 4.02 a.u.; points = number of symmetry equivalent points for that site. All numbers are in a.u.

		Madelung	Fit for EuO_6	Fit for Eu
V_{Eu}^{a}		−1.322 127 3	1.662 956[c]	−1.3222 084 2
$(\Delta V)_{max}^{b}$			3.5×10^{-4}	5.0×10^{-5}
$(\Delta V)_{av}^{c}$			2.1×10^{-7}	-2.4×10^{-5}
$\sigma(V)^{d}$			6.7×10^{-5}	2.5×10^{-5}
Site	Position	points	Fit charge for EuO_6 cluster	Fit charge for Eu cluster
O^{2-}	(0,0,1)	6		−1.998 65
Ba^{2+}	(1,1,1)	8	1.962 66	1.996 09
Nb^{5+}	(0.0,2)	6	4.970 18	4.640 23
O^{2-}	(2,0,1)	24	−1.915 79	−1.533 86
Gd^{3+}	(2,2,0)	12	1.590 02	
Ba^{2+}	(3,1,1)	24	−0.480 09	

[a] Potential at Eu^{3+} site.
[b] Largest difference between the fitted potential and the exact potential.
[c] Average difference between the fitted potential and the exact potential.
[d] Standard deviation in fitted potential.
[e] −1.322 118 5 when the contribution of six O^{2-} ions at 4.02 a.u. is included.

TABLE IV. Comparison of numerical (NMCHF), basis set (ASCF), and COSCI total energies relative to the average total energy (in a.u.).

State	NMCHF[a] (I)	ASCF[b] (II)	COSCI[c] (III)	II − I	III − II
^7F	− 0.358 73	− 0.358 83	− 0.355 93	− 0.000 10	0.002 90
^5L	− 0.225 42	− 0.225 83	− 0.224 73	− 0.000 42	0.001 10
^5K	− 0.150 29	− 0.150 66	− 0.150 14	− 0.000 37	0.000 52
^3O	− 0.138 84	− 0.139 10	− 0.138 72	− 0.000 26	0.000 38
^3N	− 0.111 07	− 0.111 47	− 0.111 23	− 0.000 41	0.000 24
^5P	− 0.110 43	− 0.110 57	− 0.110 28	− 0.000 15	0.000 29
^5S	− 0.047 81	− 0.047 50	− 0.047 46	0.000 31	0.000 05

[a] E_{av} (NMCHF) = − 10 421.679 15.
[b] E_{av} (ASCF) = − 10 421.644 89.
[c] E_{av} (COSCI) = − 10 421.644 89.

B. The Eu^{3+} impurity

From the average of configuration open shell SCF calculations we have obtained the *f* or *f*-like orbital energies, which are given in Tables V and VI. In Fig. 2 the splitting of these orbital energies due to relativistic and crystal field effects is pictorially represented. In the figure the *FD* orbital energies have been shifted upward by 0.18 a.u. The additional shift (Tables V and VI) in the embedded ion results corresponds closely to the value of the Madelung potential at the Eu^{3+} site. To explain the shift seen in the embedded cluster results also the interaction with the rest of the cluster needs to be taken into account. We find that this interaction can be fitted (using data from Tables III, V, and VI) with six effective charges of − 1.5 at the O^{2-} ion positions, or with six charges of − 2.0 at a distance of 5.3 a.u.

The COSCI results concerning the ^7F and the lower of the ^5D levels are presented in Tables VII and VIII. In Fig. 3 the *FD* data on the ^7F levels is presented in the form of density of states plots. These plots have been produced by using a convolution of a Gaussian with the discrete COSCI eigenvalues. The width of the Gaussian was chosen to match the accuracy of the calculations. In Fig. 4 the EuO_6MP *FD* COSCI results for the complete *f*-manifold are shown.

Going from the free ion to the embedded ion, certain total energy levels (depending on the symmetry) and the 4*f* orbital energies are split due to the Madelung field representing the crystal. When we include the six O^{2-} ions in the cluster together with the Madelung field of the rest of the crystal, we find that the total energy splittings are reduced significantly with respect to the embedded ion results (Fig. 3, Tables VII and VIII). This behavior, which is opposite to the behavior of the transition metal ions,[36] can be explained by the presence of the filled Eu^{3+} 5*s* and 5*p* shells. The superimposed charge distributions of these shells and the oxygen ions becomes slightly deformed. A small amount of charge is shifted from the Eu–O bond region into the regions between these bonds. This in effect reduces the electrostatic splitting of the 4*f* orbitals. Also, due to the localized nature of the 4*f* orbitals, covalent effects are not as important as in the case of transition metal ions, where they lead to an increase of the splitting.

In the nonrelativistic case, crystal field theory based on free ion orbitals yields the same splittings respectively for the many-electron ^7F level and the 4*f* orbital energy. Our embedded ion results reflect this behavior rather closely, in contrast to the embedded cluster results that show substantial deviations. This is due to changes in the detailed form of the 4*f*-like spin–orbitals. From this sensitivity it can be concluded that it is important to use "relativistic" orbitals, which deviate significantly from nonrelativistic orbitals, from the outset.

The much larger splittings calculated for the bare EuO_6^{9-} cluster should be compared with the splittings which would result from a calculation on the ion with O^{2-} ions represented by six two-point charges, not including the rest of the crystal. These splittings can be estimated from our embedded ion results by assuming that the splittings are linear in the charge of the point charges. The complete Madelung potential can approximately be fitted by six charges of − 0.865 at the O^{2-} positions,[13] so we should compare the splittings calculated using the bare cluster with the splittings calculated using the embedded ion multiplied by 2.3

TABLE V. Relative and average *NR f*-electron orbital energies (a.u.)

Level	Eu *NR*	Eu *NR*	EuO_6MP *NR*	EuO_6 *NR*
a_{2u}	0.000 00	0.000 00	0.000 00	0.000 00
t_{2u}	0.000 00	0.002 10	0.002 58	0.002 54
t_{1u}	0.000 00	0.004 20	0.005 00	0.007 33
Average	− 1.778 87	− 0.458 02	− 1.142 73	0.748 40

TABLE VI. Relative and average *FD f*-electron orbital energies (a.u.).

Level	Eu *FD*	EuMP *FD*	EuO_6MP *FD*	EuO_6 *FD*
e_{2u}	0.000 00	0.000 00	0.000 00	0.000 00
f_u	0.000 00	0.002 62	0.002 13	0.003 46
e_{2u}	0.024 10	0.023 80	0.023 80	0.023 69
f_u	0.024 10	0.026 16	0.025 63	0.026 54
e_{1u}	0.024 10	0.027 71	0.026 95	0.028 96
Average	− 1.595 26	− 0.274 29	− 0.970 88	0.923 39

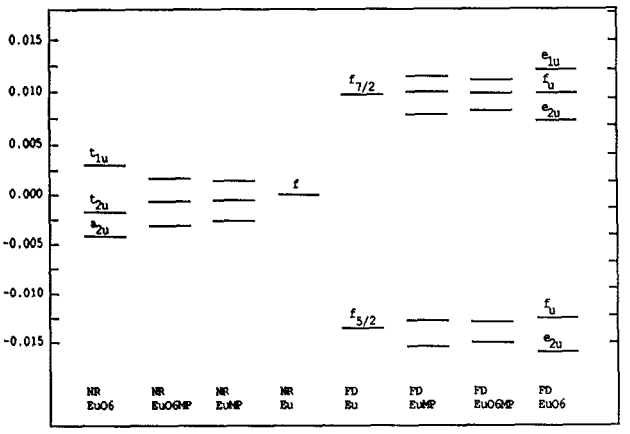

FIG. 2. Calculated splittings (in a.u.) of the orbital energies of the f and f-like orbitals due to relativistic and crystal field effects, relative to the average energies.

(= 2/0.865). Now we find a similar trend as before, inclusion of the six O^{2-} ions reduces the calculated splittings.

The differences going from embedded ion to embedded cluster are relatively large (of the same order of magnitude as the crystal field splittings), and one might ask whether the cluster should be enlarged. The distance from the Eu^{3+} ion to the next-nearest-neighbors (the Ba^{2+} ions) is rather large ($\sim$7 a.u.), and inclusion of these ions in the cluster is therefore not expected to alter the results significantly. It is expected, however, that the use of point charges deforms to oxygen charge distributions somewhat.

C. The spectrum

The dominant luminescence transitions occurring in this system are basically the atomic $^5D_0 \rightarrow {}^7F_1$ and $^5D_0 \rightarrow {}^7F_2$ transitions. The first of these is a magnetic dipole transition which can be seen clearly in the spectrum. The second transition is an induced electric dipole transition, allowed by vibronic coupling to phonon modes that break the inversion symmetry. This transition is split by the reduction of the symmetry. In Table IX the calculated transition wave numbers are given.

Based on the EuO_6MP *FD* results, we expect that the splitting of the $^5D_0 \rightarrow {}^7F_2$ transition is of the order of 100 cm^{-1}. The free tom model shows no splitting. When we introduce the Madelung potential the splitting is somewhat overestimated (251 cm^{-1}). Inclusion of the neighboring O^{2-} ions in the model (EuO_6MP) reduces the splitting to

TABLE VII. *NR* COSCI energies in a.u. of the lowest states of the f^6-manifold with their degeneracies.

	Eu *NR*		EuMP *NR*		EuO_6MP *NR*		EuO_6 *NR*	
^7F	0.000 00	49	0.000 00	21	0.000 00	21	0.000 00	21
			0.002 28	21	0.001 38	21	0.003 43	21
			0.004 52	7	0.003 17	7	0.005 10	7
^5D	0.114 78	25	0.116 07	15	0.114 07	15	0.114 72	15
			0.116 70	10	0.114 35	10	0.115 45	10

TABLE VIII. *FD* COSCI energies in a.u. of the lowest states of the f^6-manifold with their degeneracies.

	Eu *FD*		EuMP *FD*		EuO_6MP *FD*		EuO_6 *FD*	
$^7F_0$	0.000 00	1	0.000 00	1	0.000 00	1	0.000 00	1
$^7F_1$	0.001 71	3	0.001 66	3	0.001 70	3	0.001 66	3
$^7F_2$	0.004 82	5	0.003 99	2	0.004 49	2	0.004 08	2
			0.005 13	3	0.004 99	3	0.005 07	3
$^7F_3$	0.008 94	7	0.008 51	1	0.008 71	1	0.008 54	1
			0.009 17	3	0.008 94	3	0.008 94	3
			0.009 35	3	0.009 02	3	0.009 21	3
$^7F_4$	0.013 77	9	0.012 94	3	0.013 36	3	0.012 85	3
			0.014 20	2	0.013 77	2	0.014 19	2
			0.014 66	3	0.013 98	3	0.014 30	3
			0.015 08	1	0.014 24	1	0.014 41	1
$^7F_5$	0.019 10	11	0.018 66	3	0.018 76	3	0.018 57	3
			0.018 81	2	0.018 81	2	0.018 74	2
			0.019 21	3	0.019 16	3	0.018 80	3
			0.020 09	3	0.019 30	3	0.019 91	3
$^7F_6$	0.024 74	13	0.024 12	2	0.024 30	2	0.023 98	2
			0.024 25	3	0.024 33	3	0.024 11	3
			0.024 54	1	0.024 44	1	0.024 41	1
			0.026 06	3	0.024 94	3	0.025 42	3
			0.026 22	3	0.025 03	3	0.025 59	3
			0.026 37	1	0.025 11	1	0.025 73	1
$^5D_0$	0.093 70	1	0.093 83	1	0.092 24	1	0.092 18	1
$^5D_1$	0.101 21	3	0.101 32	3	0.099 72	3	0.099 61	3
$^5D_2$	0.112 75	5	0.112 63	3	0.111 15	3	0.110 84	3
			0.113 16	2	0.111 25	2	0.111 28	2

110 cm^{-1}. This number is to be compared with the number found by van Piggelen (139 cm^{-1}).[13] Although the calculated splitting is quite consistent with the experimental data, a more precise comparison cannot be made at present. The observed vibronic transitions have not been assigned and in fact more and better resolved data are required to do this.[37] The EuO_6MP model, however, should yield a reasonable description of the effects of the surroundings. We tend therefore to conclude that a crystal field model based on just the Madelung field overestimates the splitting.

The spin–orbit splitting (using the weighted average of the E_g and the T_{2g} levels) is calculated to be 628, 662, and 678 cm^{-1} for, respectively, Eu, EuMP, and EuO_6MP. This is in good agreement with the experimental data from which we estimate the splitting to be between 600 and 700 cm^{-1}. van Piggelen's results yield a somewhat larger value (804 cm^{-1}). Except for the neglect of the Breit interaction we have not introduced any approximations in the description of the relativistic effects, so we expect that our results are reliable at this point.

The calculated splitting between the ^5D level and the ^7F level is much too large, in all calculations. For the $^5D_0 \rightarrow {}^7F_1$ transition, we have a discrepancy with experiment of $\sim$3000 cm^{-1}. This large error cannot be attributed to defects of the COSCI or basis set approach (in Sec. V A we have seen that the worst of these errors is of order 600 cm^{-1}). This difference is of course to be expected at the present level of theory since most of the correlation effects have not yet been included.

VI. CONCLUSIONS

In this paper we have given results of calculations on EuO_6^{9-} clusters in a Madelung potential, as a model for an

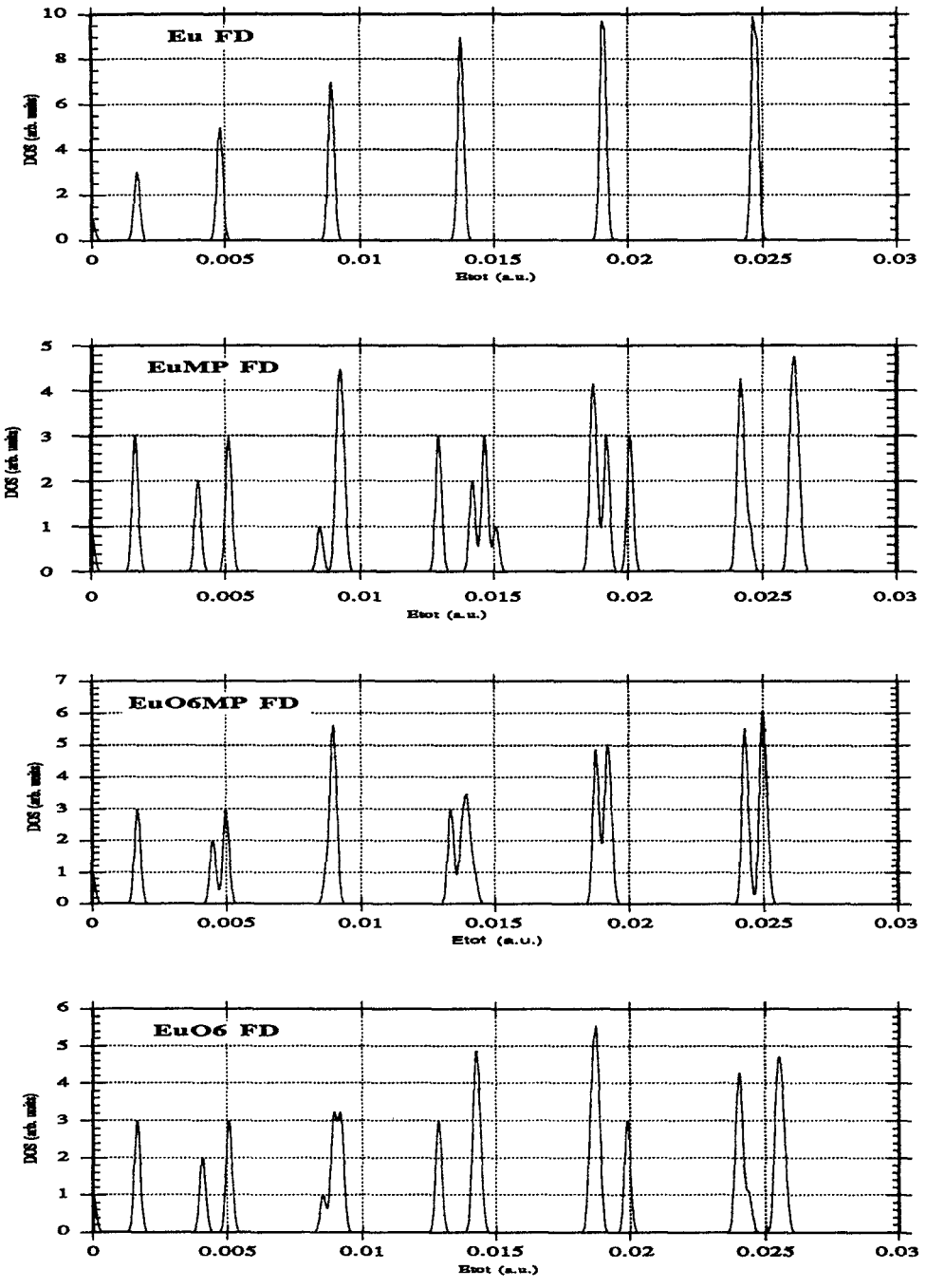

FIG. 3. Density of states from the COSCI results (^7F level shown).

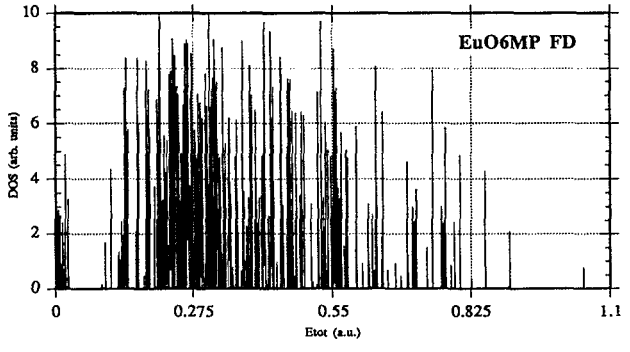

FIG. 4. Density of states from the EuO_6MP *FD* COSCI results.

Eu^{3+} impurity in the Ba_2GdNbO_6 crystal. The calculations indicate the state of the art in *ab initio* relativistic quantum chemistry, i.e., the Hartree–Fock–Dirac and COSCI formalism applied to molecules. The COSCI method has proven to be extremely useful in obtaining all the individual states of the open shell manifold.

Relativistic effect, except for the Breit interaction, the effects of the surroundings on the Eu^{3+} ion, and part of the *f*-shell configuration interaction are treated in a systematic manner. The open shell configuration interaction method employed yields an *ab initio* intermediate coupling description of the f^6-like manifold.

Our results show that the splittings due to relativistic

TABLE IX. Energies of the fluorescence transitions (in cm^{-1}).

Transition	Eu *FD*	EuMP *FD*	EuO_6MP *FD*	van Piggelen	Exp.[a]
$^5D_0 \rightarrow {}^7F_1$	20 189	20 229	19 871	20 459	16 800
$^5D_0 \rightarrow {}^7F_2\ (E_g)$	19 507	19 718	19 259	19 738	16 150[b]
$^5D_0 \rightarrow {}^7F_2\ (T_{2g})$	19 507	19 467	19 149	19 599	16 150[b]

[a] Blasse *et al.* (Refs. 28 and 29).

[b] Unweighted average of the six lines observed in this region. The separation between the lines is $\sim 100\ cm^{-1}$.

effects, which are much larger than the splittings due to the surroundings, can be calculated with an accuracy of $\sim 10\ cm^{-1}$. We have also found that both a pure Madelung field and a bare EuO_6^{9-} cluster significantly overestimate the splittings introduced by the surroundings. It is clear from our nonrelativistic results that the detailed form of the orbitals is important in the calculation of these splittings. Hence the preferred approach should be to use relativistic orbitals from the outset.

A significant discrepancy with experiment is found where splittings between Russell–Saunders terms are concerned (as in the luminescence spectra). This discrepancy, which is also present on the atomic level, is due to the neglect of most of the correlation effects and does not differ much from the discrepancies found in nonrelativistic calculations.

ACKNOWLEDGMENTS

This investigation was supported by The Netherlands Foundation for Chemical Research (SON), the Netherlands Foundation for Fundamental Research on Matter (FOM), and the National Computing Facilities Foundation (NCF) with financial aid from the Netherlands Organization for Scientific Research (NWO).

[1] J. Becquerel, Z. Phys. **58**, 205 (1929).
[2] H. Bethe, Ann. Phys. **3**, 135 (1929).
[3] B. T. Thole, G. van der Laan, J. C. Fuggle, G. A. Sawatzky, R. C. Karnatak, and J.-M. Esteva, Phys. Rev. B **32**, 5107 (1985).
[4] B. T. Thole, G. van der Laan, and G. A. Sawatzky, Phys. Rev. Lett. **55**, 2086 (1985).
[5] K. Balasubramanian and K. S. Pitzer, in *Ab initio Methods in Quantum Chemistry*, edited by I. K. P. Lawley (Wiley, New York, 1987), p. 287.
[6] P. Pyykkö, Chem. Rev. **88**, 563 (1988).
[7] P. Pyykkö, Adv. Quantum. Chem. **11**, 353 (1978).
[8] P. A. Christiansen, W. C. Ermler, and K. S. Pitzer, Ann. Rev. Phys. Chem. **36**, 407 (1985).
[9] P. J. C. Aerts, thesis, Groningen, 1986.
[10] P. J. C. Aerts and W. C. Nieuwpoort, Int. J. Quantum Chem. Symp. **19**, 267 (1986).
[11] O. Visser, L. Visscher, P. J. C. Aerts, and W. C. Nieuwpoort, Theor. Chim. Acta (to be published).
[12] K. G. Dyall, P. R. Taylor, K. Faegri, Jr., and H. Partridge, J. Chem. Phys. **95**, 2583 (1991).
[13] H. U. van Piggelen, thesis, Groningen, 1978.
[14] O. Visser, P. J. C. Aerts, and L. Visscher, in *The Effects of Relativity in Atoms, Molecules and the Solid State*, edited by I. P. Grant, B. Gyorffy, and S. Wilson (Plenum, New York, 1990).
[15] L. Visscher, P. J. C. Aerts, and O. Visser, in *The Effects of Relativity in Atoms, Molecules and the Solid State*, edited by I. P. Grant, B. Gyorffy, and S. Wilson (Plenum, New York, 1990).
[16] P. A. M. Dirac, Proc. R. Soc. London Ser. A **117**, 610 (1928).
[17] P. A. M. Dirac, Proc. R. Soc. London Ser. A **118**, 351 (1928).
[18] I. P. Grant and H. M. Quiney, Adv. At. Mol. Phys. **23**, 37 (1988).
[19] G. Breit, Phys. Rev. **34**, 553 (1929).
[20] H. M. Quiney, I. P. Grant, and S. Wilson, J. Phys. B **23**, L271 (1990).
[21] S. Okada, M. Shinada, and O. Matsuoka, J. Chem. Phys. **93**, 5013 (1990).
[22] C. C. J. Roothaan, Rev. Mod. Phys. **32**, 179 (1960).
[23] R. E. Stanton and S. J. Havriliak, Chem. Phys. **81**, 1910 (1984).
[24] P. J. C. Aerts and W. C. Nieuwpoort, Chem. Phys. Lett. **125**, 83 (1986).
[25] W. Kutzelnigg, Int. J. Quantum Chem. **25**, 107 (1984).
[26] R. C. Raffenetti, J. Chem. Phys. **58**, 4452 (1973).
[27] G. Blasse, A. Bril, and W. C. Nieuwpoort, in *Proceedings of the International Conference on Luminescence*, edited by G. Szigeti (Akad. Kiado, Budapest, 1966), p.1646.
[28] G. Blasse and A. Bril, Philips Tech. Tijdscrift **31**, 314 (1970).
[29] B. R. Judd, Phys. Rev. **127**, 750 (1962).
[30] C. S. Ofelt, J. Chem. Phys. **37**, 511 (1962).
[31] F. Galasso and W. Darby, J. Phys. Chem. **66**, 131 (1962).
[32] J. Almlöf and U. Wahlgren, Theor. Chim. Acta **28**, 161 (1973).
[33] H. U. van Piggelen, W. C. Nieuwpoort, and G. A. van der Velde, J. Chem. Phys. **72**, 3727 (1980).
[34] R. Broer (unpublished) (see Table I).
[35] C. Froese-Fischer, *The Hartree–Fock Method for Atoms* (Wiley, New York, 1977).
[36] A. J. H. Wachters and W. C. Nieuwpoort, Int. J. Quantum Chem. **5**, 391 (1971).
[37] J. P. Morley, T. R. Faulkner, and F. S. Richardson, J. Chem. Phys. **77**, 1710 (1982).